

# Early structure formation in quintessence models and its implications for cosmic reionisation from first stars

U. Maio<sup>1,2</sup>, K. Dolag<sup>1</sup>, M. Meneghetti<sup>3,4</sup>, L. Moscardini<sup>2,5</sup>, N. Yoshida<sup>6</sup>, C. Baccigalupi<sup>3,7,8</sup>,  
M. Bartelmann<sup>3</sup>, F. Perrotta<sup>3,7,8</sup>

<sup>1</sup> Max-Planck Institut fuer Astrophysik, Karl-Schwarzschild Strasse 1, D-85748 Garching, Germany (maio,kdolag@mpa-garching.mpg.de)

<sup>2</sup> Dipartimento di Astronomia, Università di Bologna, via Ranzani 1, I-40127 Bologna, Italy (lauro.moscardini@unibo.it)

<sup>3</sup> Zentrum für Astronomie, ITA, Universität Heidelberg, Albert-Überle-Straße 2, D-69120 Heidelberg, Germany (meneghetti,mbartelmann@ita.uni-heidelberg.de)

<sup>4</sup> INAF, Osservatorio Astronomico di Bologna, via Ranzani 1, I-40127 Bologna, Italy

<sup>5</sup> INFN, Sezione di Bologna, viale Berti Pichat 6/2, I-40127 Bologna, Italy

<sup>6</sup> Department of Physics, Nagoya University, Nagoya, Aichi 464-8602, Japan (nyoshida@phys.nagoya-u.ac.jp)

<sup>7</sup> SISSA/ISAS, via Beirut 4, I-34014 Trieste, Italy (bacci,perrotta@sissa.it)

<sup>8</sup> INFN, Sezione di Trieste, via Valerio 2, I-34127 Trieste, Italy

Accepted ????. Received ???; in original form July 2006

## ABSTRACT

We present the first hydrodynamic N-body simulations of primordial gas clouds responsible for the reionisation process in dark energy cosmologies. We compare the cosmological constant scenario with a SUGRA quintessence model with marked dynamics in order to highlight effects due to the different acceleration histories imposed by the dark energy. We show that both the number density of gas clouds and their clumpiness keep a record of the expansion rate during evolution, similar to the non-linear dark matter profile at virialisation, as was recently demonstrated by Dolag et al. (2004). Varying the shape of the primordial power spectrum, we show how this effect is mitigated by a running spectral index decreasing the power at small scales. Our results demonstrate that, in order to constrain the dark energy from large scale structures, one must track its effects down to the distribution of luminous matter.

**Key words:** early universe – cosmology: theory – galaxies: formation

## 1 INTRODUCTION

Different observational data, like those from high-redshift supernovae (Riess et al. 2004; Astier et al. 2006), the cosmic microwave background (Spergel et al. 2003, 2006), and large-scale structure (Tegmark et al. 2004; Cole et al. 2005), are now giving a consistent picture of our universe, which can be described by the so-called ‘concordance’  $\Lambda$ CDM model: a spatially flat universe whose expansion accelerates in the present epoch because of a dominant dark energy component. Historically, the first and simplest candidate for that has been the cosmological constant  $\Lambda$ , corresponding to matter with an equation of state  $p = w\rho c^2$ , with constant  $w = -1$ . However, observations suggest a value for  $\Lambda$  which is more than a hundred orders of magnitude smaller than the energy scales expected to be responsible in the very early universe.

To avoid inelegant solutions based on parameter fine-tuning, the general idea of dark energy is extended to encompass the so-called quintessence, possibly corresponding to a suitably self-interacting scalar field, whose pressure and energy density evolve during cosmic history. The currently available observational data sets do not allow yet to place strong constraints on  $w$ . We know that it has to come close to  $-1$  with a precision of about 10 per cent at the present epoch (see, e.g., Riess et al. 2004; Spergel et al. 2006),

but its redshift evolution is still poorly constrained and can hopefully be determined only with new-generation data; see Seljak et al. (2005) for one of the very first attempts to measure the high-redshift dark energy equation of state.

One consequence of  $w > -1$  earlier is that the formation of cosmic structures sets in earlier compared to the  $\Lambda$ CDM model. At a given redshift, this corresponds to a higher abundance of more concentrated halos (see, e.g., Dolag et al. 2004). This may open alternative ways to study quintessence models based on galaxy-cluster counts (Wang & Steinhardt 1998; Haiman et al. 2001; Battye & Weller 2003; Majumdar & Mohr 2003) and strong gravitational lensing (Bartelmann et al. 2003; Meneghetti et al. 2005).

The different history of structure formation must also affect the reionisation epoch. To produce the required ionising radiation, a sufficiently high number of early stellar sources is needed, such as super-massive Pop-III stars or more ‘standard’, massive Pop-II stars in proto-galaxies. In particular, Pop-III stars are supposed to be composed mainly of hydrogen and helium with their primordial abundances, to have masses  $\gtrsim 100 M_{\odot}$  much larger than the standard Pop-I and -II stars, and to form in dark matter haloes with typical masses of  $10^{5\cdots 6} M_{\odot}$  (the so-called mini-haloes).

The recent analysis of the temperature-polarisation cross-correlation and the polarisation auto-correlation measured by the WMAP satellite now allows the estimation of the epoch when reionisation occurs. The Thomson optical depth of  $\tau \sim 0.17 \pm 0.04$  extracted from the first-year WMAP data had been interpreted as signalling the high redshift of  $z = 17 \pm 5$  for the primordial epoch of global reionisation (Kogut et al. 2003). The recently released three-year WMAP data allowed an improved control in particular of the polarised foreground emission, yielding  $\tau = 0.09 \pm 0.03$ . This corresponds to  $z = 10_{-2.3}^{+2.7}$  for the completion of the reionisation process, even if some level of parameter degeneracy still remains (see, e.g., Fig. 3 in Spergel et al. 2006).<sup>1</sup> Different authors (see, e.g., Wyithe & Loeb 2003; Ciardi et al. 2003; Sokasian et al. 2003, 2004) suggested that these reionization data can place new complementary constraints on the cosmological parameters, and in particular on the nature of dark energy.

So far, studies of the structure formation process in dark energy cosmologies were focused on modifications of dark matter structures due to the different expansion histories (see, e.g., Klypin et al. 2003; Dolag et al. 2004). They revealed that virialised objects keep a record of the expansion rate at the time of their formation. The general picture is that in cosmologies with  $w > -1$ , the increase of the dark energy density with redshift enhances structure growth, and virialised haloes become more concentrated because of the denser environment they form in (Dolag et al. 2004). This effect is stronger in tracking quintessence models, which we describe in the next section, in which the increase of the dark energy density with redshift is enhanced. Complementary hydrodynamical simulations still need to be carried out. This work is a first step into this direction, beginning with the numerical study of the dependence of the primeval gas clouds responsible for the reionisation process on the cosmic expansion rate at their formation time.

Due to the higher concentration of structures in dark energy scenarios, which has so far been verified only for the dark matter, it is mandatory for our study to control the shape of the primordial power spectrum. When combined with the Ly- $\alpha$  forest data and with the analysis of the  $2dF$  galaxy redshift survey, the first-year WMAP results supported a “running” spectral index which tilts the spectrum slightly towards small scales, starting at  $k \gtrsim 1 \text{ Mpc}^{-1}$ . The three-years WMAP data are compatible with this (Spergel et al. 2006), albeit with less emphasis than the earlier results. A running index would cause a slower growth and evolution of small-scale cosmic structures compared to models with a constant index  $n$ . A reduction of power on small scales may alleviate several potential discrepancies in the  $\Lambda$ CDM model, such as the abundance of substructures in galaxies and the high central concentration of galactic haloes. However, as shown by analytic and numerical work (see, e.g. Somerville et al. 2003; Yoshida et al. 003b), models with a running spectral index (RSI) may have severe problems in producing enough objects to allow a global reionisation at high redshift. Since this might be balanced by the enhanced structure growth due to the dark energy, it is important to jointly study these two aspects.

In the present paper, we study the high-redshift structure formation in quintessence models based on the results of high-resolution cosmological N-body simulations combined with hydro-

dynamics. Specifically, we consider four different cases combining two flat cosmological models, i.e. the concordance  $\Lambda$ CDM model and a quintessence model with a SUGRA potential, with two types of the primordial power spectrum, one with a constant spectral index  $n = 1$  and an RSI model assuming the best fit relation found by Spergel et al. (2003). More detail will be given in the next section. The paper is organised as follows. In Sect. 2, we describe the general characteristics of the hydrodynamical simulations used below and introduce the quintessence models chosen. The techniques adopted for identifying dark matter haloes and the corresponding results are presented in Sect. 3. The abundances of gas clouds are presented in Sect. 4 together with the clumping factors and recombination times as computed from the simulation outputs. The implications of the previous results in terms of reionisation are discussed in Sect. 5. The final discussion and our main conclusions are drawn in Sect. 6.

## 2 THE SIMULATIONS

We first review the cosmologies chosen, and then the computational and hydrodynamical features of our numerical simulations. As mentioned in the introduction, this work is a first step towards investigating the dependence of hydrodynamic N-body simulated structures on the global cosmic expansion rate, and it is appropriate to study the connection with the shape of the primordial power spectrum. Thus, we need dark energy cosmologies with different dynamics as well as constant and running index in the primordial power spectrum.

The standard, concordance  $\Lambda$ CDM model is our reference case. It is spatially flat, has the present matter density  $\Omega_{0m} = 0.3$ , the baryon density  $\Omega_{0b} = 0.04$ , and a dominating cosmological constant,  $\Omega_{0\Lambda} = 0.7$ . The Hubble constant is assumed to be  $h = 0.7$  in units of  $100 \text{ km s}^{-1} \text{ Mpc}^{-1}$ . The second model is chosen so as to emphasise the dynamical effects of the dark energy. The spatial curvature is also vanishing, with  $\Omega_{0m} = 0.3$  and 70 per cent of the critical density contributed by a quintessence scalar field  $\Phi$  evolving in time under the effect of a potential energy  $V(\Phi)$ . We review here the main characteristics of this model, referring to Peebles & Ratra (2003) and references therein for further detail.

The field  $\Phi$  must satisfy the Klein-Gordon equation

$$\ddot{\Phi} + 3H\dot{\Phi} + \frac{\partial V}{\partial \Phi} = 0. \quad (1)$$

The equation-of-state parameter  $w \equiv p/(\rho c^2)$  is

$$w = \frac{\frac{1}{2}\dot{\Phi}^2 - V(\Phi)}{\frac{1}{2}\dot{\Phi}^2 + V(\Phi)}. \quad (2)$$

Evidently,  $w$  evolves with redshift, but the behaviour of the cosmological constant is reproduced as  $w \rightarrow -1$  in the static limit  $\dot{\Phi}^2 \ll V(\Phi)$ .

The attractive feature of such models are their attractor solutions which exist for exponential and inverse power law potentials or combinations of those. Suitably tuning the potential amplitude, they can reach the present level of dark energy starting from a large range of initial conditions. The evolution of the equation of state may be more or less pronounced along these trajectories. We wish to have pronounced dark-energy dynamics in order to clearly identify its effects. Thus, we choose a SUGRA potential

$$V(\Phi) = \frac{M^{4+\alpha}}{\Phi^\alpha} \exp(4\pi G\Phi^2), \quad (3)$$

<sup>1</sup> We have also to notice that the three-year WMAP data are suggesting a lower value not only for  $\tau$ , but also for the power spectrum normalization  $\sigma_8$ : these two effects nearly cancel in terms of early structure formation, i.e. the inferred small  $\tau$  does not really allow slow reionization for a given  $\sigma_8$ .

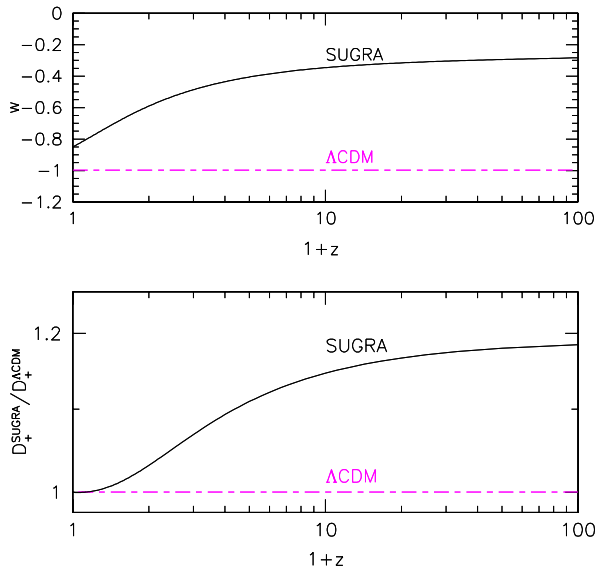


**Figure 1.** *Upper panel:* The redshift evolution of the equation-of-state parameter  $w$  for the SUGRA model with  $w_0 = -0.85$  (solid line), compared to the concordance  $\Lambda$ CDM model (dash-dotted line). *Lower panel:* The linear growth factor (normalised to the  $\Lambda$ CDM model at present) for the same cosmologies as in the upper panel.

where  $G$  is the Newton constant, as suggested by super-gravity corrections (Brax & Martin 1999, 2000). By exploiting the properties of tracking trajectories, we fix  $M$  by requiring that the dark energy makes up 70 per cent of the critical density today, and  $\alpha = 6.5$  so that  $w \rightarrow w_0 \equiv w(z=0) = -0.85$  today. At higher redshift,  $w > w_0$  (Brax & Martin 2000), which meets our purpose of emphasising differences with the  $\Lambda$ CDM model. It should be noted that this model is already at variance with the observational constraints (see, e.g., Spergel et al. 2003; Knop et al. 2003; Riess et al. 2004).

The upper panel of Fig. 1 shows the redshift evolution of  $w$  for this model. The differences with the standard  $\Lambda$ CDM model (constant  $w = -1$ ) are large at all redshifts. In particular, during the epoch of reionisation which we are mostly interested in, the SUGRA model has  $w \approx -0.35$ . Notice that  $w$  strongly affects the formation history of cosmic structures through its modified expansion history. This is evident from the lower panel in Fig. 1, which shows the linear growth factor (normalised to coincide with the  $\Lambda$ CDM model at  $z=0$ ) for the model shown above. In quintessence models where the dark energy is more abundant in the past with respect to now, structures tend to form earlier if the perturbation power spectrum is normalised at the present epoch. This is due to the earlier dark energy dominance, slowing down the perturbation growth. In our SUGRA model with  $w_0 = -0.85$ , fluctuations at  $z = 20$  are expected to be  $\approx 15$  per cent higher than in the  $\Lambda$ CDM model. Consequently, we expect that non-linearity to be reached earlier, with obvious consequences for the reionisation epoch.

Dynamical dark energy generally increases the concentration of virialised structures (Dolag et al. 2004), which can also be caused by a modified primordial power spectrum. Therefore, we vary the simulation set-up using two different shapes of the primordial power spectrum. Specifically, for both cosmological models ( $\Lambda$ CDM and SUGRA), we construct initial conditions corre-

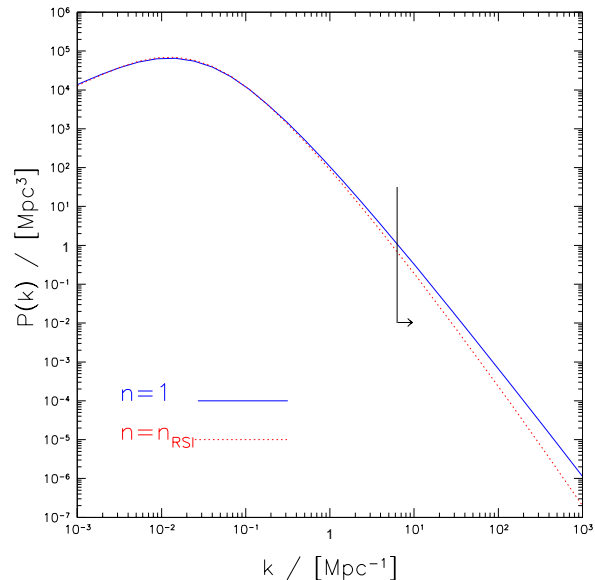


**Figure 2.** Comparison between the two different CDM power spectra adopted in generating the initial conditions for the numerical simulations: solid and dotted lines show spectra with fixed  $n = 1$  and with the running spectral index (4), respectively. The arrow indicates the range of length scales covered by our simulations.

sponding to two scenarios, namely a power spectrum with the standard constant  $n = 1$  normalised to  $\sigma_8 = 0.9$ . The second model also has  $\sigma_8 = 0.9$ , but allows for a reduced primordial power on small scales as suggested by the combined analysis of the first-year WMAP data, galaxy surveys and Ly- $\alpha$  data (see, e.g. Spergel et al. 2003), within the range compatible with the three-year WMAP data (Spergel et al. 2006).

The case for a running spectral index is interestingly controversial. Re-analyses of the Ly- $\alpha$  data (see, e.g. Viel et al. 2004; Seljak et al. 2005; Viel & Haehnelt 2006; Zaroubi et al. 2006) lend much less support for a running spectral index than reported based on the first-year WMAP data and favour a constant primordial spectral index very close to unity (see, however, Desjacques & Nusser 2005). On the other hand, a running spectral index is still viable and fits the three-year WMAP data well (Spergel et al. 2006), while the support of a pure power law from large scale structures persists (see, e.g., Viel et al. 2006; Seljak et al. 2006). As mentioned before, we choose our cosmological models so as to cover a broad range of phenomenologies rather than to fit the existing data well. Thus, we choose to adopt a primordial power spectrum given by  $P(k) \propto k^{n(k)}$ , with

$$n(k) = n(k_0) + \frac{1}{2} \frac{dn}{d \ln k} \ln \left( \frac{k}{k_0} \right), \quad (4)$$

where  $k_0 = 0.05 \text{ Mpc}^{-1}$ ,  $n(k_0) = 0.93$  and

$$\frac{dn}{d \ln k} = -0.03. \quad (5)$$

This choice conveniently allows a direct comparison with the similar analysis by Yoshida et al. (003b), who adopt the same primordial power spectrum, but only consider the concordance  $\Lambda$ CDM model. It is worth recalling that this represents the best fit to the first-year WMAP data and remains compatible with the three-year data,  $dn/d \ln k \lesssim -0.06$  (Spergel et al. 2003, 2006). Figure 2 shows the two primordial power spectra considered here. Evidently,

they differ at large  $k$  where the RSI spectrum is steeper. Less power on small scales will delay the structure formation (see also the corresponding discussion in Yoshida et al. 003b).

Combining two cosmological models ( $\Lambda$ CDM and SUGRA) with two primordial power spectra (constant  $n = 1$  and RSI), we ran four different simulations;  $\Lambda$ CDM and SUGRA with  $n = 1$  and  $\Lambda$ CDM-RSI and SUGRA-RSI with a running spectral index. The initial conditions were generated at  $z \approx 120$  using a comoving periodic box of 1 Mpc side length. We followed Dolag et al. (2004) in adapting the initial conditions for  $\Lambda$ CDM to those for the SUGRA model. Thus, by construction, only the pairs of models sharing the same primordial power spectrum have the same random phases, allowing a direct comparison of the structures formed. The models with different primordial power spectra have different random phases and can thus not be directly compared (see Fig.3).

Since we are interested in structures during cosmic reionisation, the box size used here can be considered sufficiently large to suppress cosmic variance (see the discussion on effects of finite box sizes in Yoshida et al. 003b; Bagla & Prasad 2006). Moreover, to prevent the non-linear regime from reaching the fundamental fluctuation mode in the simulations, we stopped the simulation at the latest at  $z \sim 15$ .

When the gas starts cooling significantly within the first forming structure, the simulation time step can become very small (since we neglect feedback in these simulations), effectively stopping the simulation. Accordingly, we had to stop some simulations at a higher redshift, for example the SUGRA simulation, which could only be evolved until  $z \sim 19$  because of its more rapid evolution, as we shall see in the later analysis. Nonetheless, all simulations are followed long enough for them to form the sufficient amount of structure we need for our analysis.

The simulations were performed using the GADGET2 code (Springel et al. 2001; Springel 2005) on the IBM-SP4/5 at CINECA (Bologna). GADGET2 is based on the combination of a tree-particle-mesh algorithm to solve the gravitational forces, and the smoothed particle hydrodynamics (SPH) scheme to describe the hydrodynamics of gas particles. The code follows the non-equilibrium reactions of different chemical species ( $e^-$ ,  $H$ ,  $H^+$ ,  $H^-$ ,  $He$ ,  $He^+$ ,  $He^{++}$ ,  $H_2$ ,  $H_2^+$ ), using the reaction coefficients computed by Abel et al. (1997) (for more detail, see also Anninos et al. 1997; Yoshida et al. 003a), and adopts the cooling rate due to molecular hydrogen estimated by Galli & Palla (1998). The density field was sampled with  $324^3$  dark matter (DM) particles and an equal number of gas particles, having a mass of  $\sim 1040 M_\odot$  and  $160 M_\odot$ , respectively. The comoving Plummer-equivalent gravitational softening length was fixed to  $\epsilon = 0.143$  kpc.

In Fig. 3 we show the projected gas and (mass-weighted) temperature distributions for all four models at  $z = 20.6$ . As expected, the RSI simulations appear delayed, exhibiting smoother density and temperature distributions. The SUGRA models reveal their expected behaviour with a more evolved density field than their  $\Lambda$ CDM counterparts. Since the models with and without RSI have different random phases in their initial conditions, they are not supposed to reproduce the same structures.

### 3 THE ABUNDANCE OF DARK MATTER HALOES

The abundance of virialised dark matter haloes is usually expressed by the mass function  $N(M)$ . From a theoretical point of view, different relations are available to predict the redshift evolution

of  $N(M)$  once the cosmological model is fixed. Some of these were obtained from a specific model for the collapse of structures (Press & Schechter 1974; Sheth & Tormen 2002); in other cases, they represent best fits to N-body simulations with very high resolution (Sheth & Tormen 1999; Jenkins et al. 2001; Warren et al. 2006). However, the theoretical mass functions have not yet been extensively tested in the regime of very low masses and very high redshifts which we are mainly interested in, where their predictions differ by orders of magnitude. This is due to the difficulty of combining sufficient resolution in space and mass with regions large enough to be considered a fair samples of our universe.

The existing studies yield contradictory results. Simulations covering large volumes, such as those presented in Reed et al. (2003) ( $432^3$  particles in a  $50 h^{-1}$  Mpc box) and in Springel et al. (2005) ( $2160^3$  particles in a  $500 h^{-1}$  Mpc box), found that the (Sheth & Tormen 1999, hereafter ST99) formula fairly reproduces the numerical results, but they can safely identify haloes with masses  $\gtrsim 10^{10} M_\odot$  at  $z \lesssim 10$ . At  $z = 15$ , Reed et al. (2003) found a slight tendency of the ST99 model to over-predict the halo counts.

Numerical work based on much smaller boxes, such as Jang-Condell & Hernquist (2001) ( $128^3$  particles in a  $1 h^{-1}$  Mpc box) or Yoshida et al. (003b,c) ( $2 \times 324^3$  particles in a  $1 h^{-1}$  Mpc box), found very good agreement with the predictions of the (Press & Schechter 1974, hereafter PS74) model. Notice that these simulations are more affected by their finite box size (see the following discussion). Further support for the PS74 formalism at high redshifts is provided by the analysis of Gao et al. (2005), who showed that the extended Press-Schechter theory (Bond et al. 1991) correctly predicts the structure growth and the dependence of halo abundances on the density of the surrounding region in the redshift range between 50 and 30. One of the best compromises between mass resolution and volume coverage was achieved by Heitmann et al. (2006), who used an extended set of simulations with  $256^3$  particles in boxes sized between  $(4 \dots 126) h^{-1}$  Mpc. Their mass function at high redshift turns out to deviate significantly from the PS74 prediction for  $M > 10^7 h^{-1} M_\odot$ , while the agreement with the (Warren et al. 2006, hereafter W06) relation is better. Notice that the W06 formula predicts a substantial suppression of the halo abundance in the high-mass regime compared to the ST99 model. Finally, using an array of high-resolution N-body simulations with box sizes in the range  $1 - 3000 h^{-1}$  Mpc, Reed et al. (2006) recently determined the mass function of dark matter haloes at redshifts between 10 and 30. They found that the PS74 models gives a poor fit at all epochs, while the ST99 model gives a better match to the simulations, but still overpredicts the abundance of most massive objects by up to 50 per cent.

We identify dark matter haloes in our simulations by running a friends-of-friends algorithm on the dark matter particles only and setting the linking length to 20 per cent of the mean inter-particle separation. The resulting mass of each halo is then corrected by the factor  $(1040 + 160)/1040 \approx 1.15$  to account for the additional contribution by the gas particles. Figure 4 displays the redshift evolution of the number of haloes with masses exceeding  $7 \times 10^5 M_\odot$  for all four simulations. The figure compares the results with the predictions of the PS74, the ST99 and the W06 models, indicated by solid, dashed and dot-dashed lines, respectively. Note that we do not consider the relation found by Jenkins et al. (2001) because it cannot extrapolate to the mass and redshift ranges considered here.

At first sight, the dark energy dynamics as well as the modified initial power spectrum generate significant differences. First, as expected, the number of massive haloes is always lower in the RSI

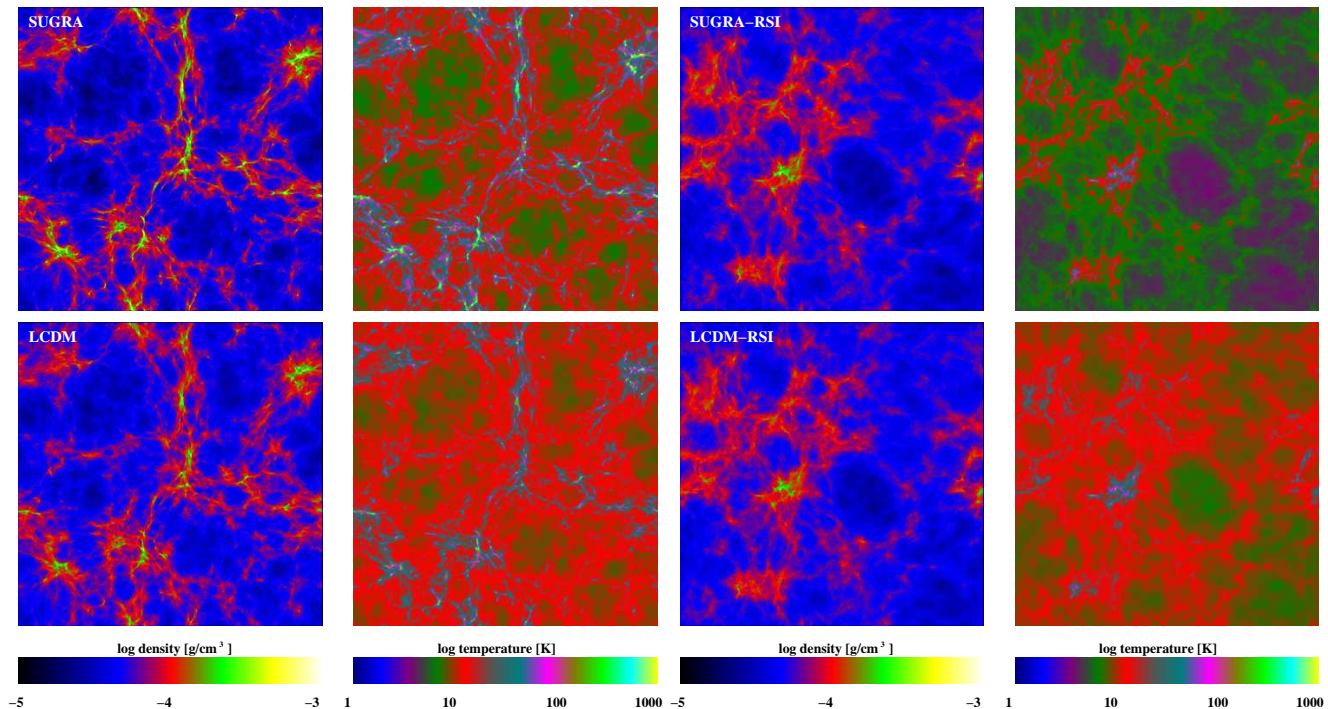


**Figure 3.** The logarithm of the projected gas-density and mass-weighted temperature at  $z = 20.6$  is shown in thin slices (1/7th of the box height) for the different models: SUGRA,  $\Lambda$ CDM, SUGRA-RSI and  $\Lambda$ CDM-RSI, as labelled in the maps. The density is in physical units and the slices are 6.6 (physical) kpc thick at  $z = 20.6$ . Note that the models with and without RSI have different random phases in their initial conditions and are thus not supposed to reproduce the same structures.

models than in their scale-invariant counterparts. While the first objects with  $M > 7 \times 10^5 M_\odot$  start appearing near  $z \simeq 30$  in the SUGRA and the  $\Lambda$ CDM simulations, this is delayed to  $z \simeq 25$  and  $z \simeq 20$  for SUGRA-RSI and  $\Lambda$ CDM-RSI, respectively.

Second, the different expansion histories leave clear records in the structure population. Considering models with the same primordial power spectrum, the halo abundance is always larger in the SUGRA than in the  $\Lambda$ CDM models by a factor  $\simeq 2$ , confirming the earlier structure formation in dynamical quintessence models expected from the modified linear growth factor in Fig. 1.

We now consider the difference to the theoretical expectations from the PS74, ST99 and W06 mass functions. All analytic relations were modified so as to account for the different expansion histories and initial power spectra in the different cosmological models. For the two simulations with a cosmological constant ( $\Lambda$ CDM and  $\Lambda$ CDM-RSI), the results indicate that the W06 formula agrees better with the simulations than the ST99 and PS74 formulae. Some small deviations are seen at very high redshifts where, however, counts are low and the statistical uncertainty is high. The ST99 mass function tends to slightly overestimate the simulation results, again mainly at high redshift, where the discrepancies with W06 are more evident. On the contrary, the PS74 mass function always underestimates the halo abundances, with differences reaching up to a factor  $\sim 3$ . Thus, our results for the cosmological-constant models agree with the previous analyses by Reed et al. (2003), Springel et al. (2005) and Heitmann et al. (2006). However, this conclusion is in conflict with other studies (Jang-Condell & Hernquist 2001; Yoshida et al. 003b,c).

The situation is different for both SUGRA models. The mass function in the simulation with constant  $n = 1$  is always larger than all theoretical predictions. In particular, the ST99 and W06 relations give very similar estimates which fall below the simulation

results by 30 per cent, while the difference with PS74 is always a factor of 3-4. The tendency of PS74 to underestimate the numerical mass function is also confirmed for SUGRA-RSI (a factor of 3-5 everywhere), while the agreement for W06 and mostly for ST99 is substantially better. The deviations reach 20 per cent only at low redshift. These results show that caution must be applied when applying the standard theoretical mass functions to very high redshift in quintessence models.

We must finally remark that, owing to the much higher mass resolution, the mass range covered in our simulations is quite different compared to earlier work. At the same time, our results could be affected by the small box size. In fact, as discussed in Yoshida et al. (003b), the “effective” variance, i.e. the amount of power on the scales covered by the simulation, can be significantly smaller than that obtained by integrating the power over all scales. This difference can systematically delay structure formation and possibly cause the discrepancies between the simulation results from different box sizes. To quantify the effect of the finite box, we apply the analytic expressions proposed by Bagla & Prasad (2006), which allow an evaluation of the required correction to the mass function. For example, assuming the PS74 approach and the redshift range covered by the data shown in Fig. 4, we find that the correction for  $M = 7 \times 10^5 M_\odot$  leads to a slight underestimate of 10-15 per cent, which does not significantly affect our previous results. Similar conclusions can be reached on the ST99 relation.

#### 4 THE PROPERTIES OF THE GAS DISTRIBUTION

We now show our results on the statistics and the physical properties of the gas distribution. We concentrate on two aspects, namely the formation time of the gas clouds and their clumping factor, fo-

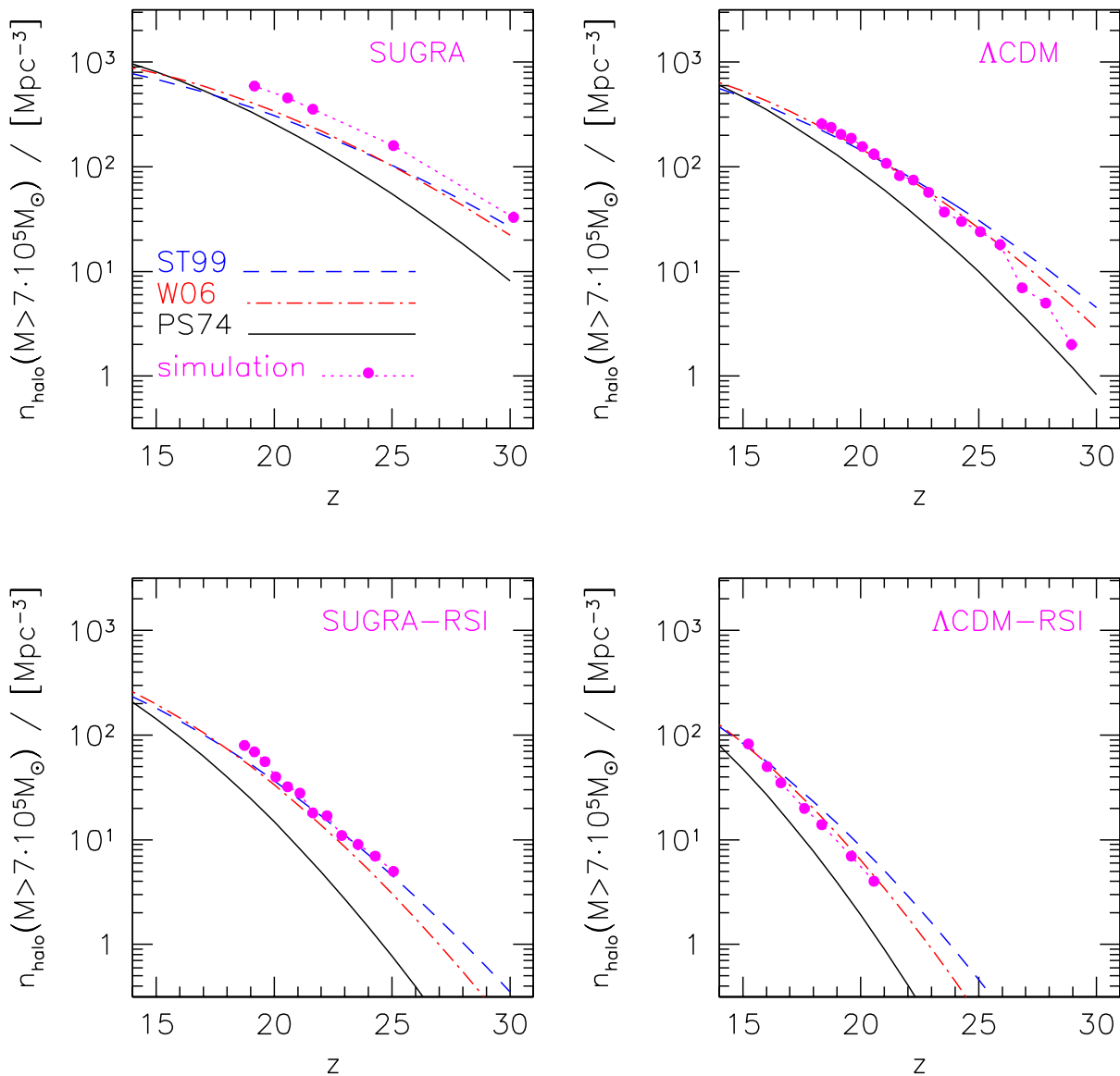


**Figure 4.** Number of haloes with mass exceeding  $7 \times 10^5 M_{\odot}$  per unit comoving volume as function of redshift in the different simulations (filled circles and dotted lines): SUGRA (upper left panel),  $\Lambda$ CDM (upper right panel), SUGRA-RSI (lower left panel),  $\Lambda$ CDM-RSI (lower right panel). Theoretical predictions based on the Press & Schechter (PS74, solid line), Sheth & Tormen (ST99, dashed line) and the Warren et al. (W06, dot-dashed line) relations are shown as well.

cusing on their dependence on the underlying dark energy cosmology and primordial power.

#### 4.1 The formation of gas clouds

We first study the formation of the gas clouds which are responsible for reionisation. For this purpose, we run a friends-of-friends algorithm to group cold and dense gas particles, assuming a linking length of 1/20th of the mean inter-particle separation to locate the densest gas concentrations. Following Yoshida et al. (003b,c), we only consider clouds exceeding  $3000 M_{\odot}$ , which corresponds to groups with at least 19 gas particles in our simulations.

The results are shown in Fig. 5 in terms of the redshift evolution of the number of gas clouds  $n_{\text{clouds}}$  identified in the four simulations. It is not surprising that the trend between the models is similar as for the dark matter haloes in Fig. 4. Gas clouds start forming earlier and are more abundant in the SUGRA than in the  $\Lambda$ CDM model with the same primordial power spectrum.

The suppression of power on small scales is, however, the dominant effect. In fact, the two RSI models have their structure formation delayed and have the smallest number of gas clouds in the final outputs. At  $z \simeq 19$ , there are order-of-magnitude differences between the models. We find  $\sim 300$  clouds for SUGRA,  $\sim 50$  for  $\Lambda$ CDM, 7 for SUGRA-RSI and no clouds for  $\Lambda$ CDM-

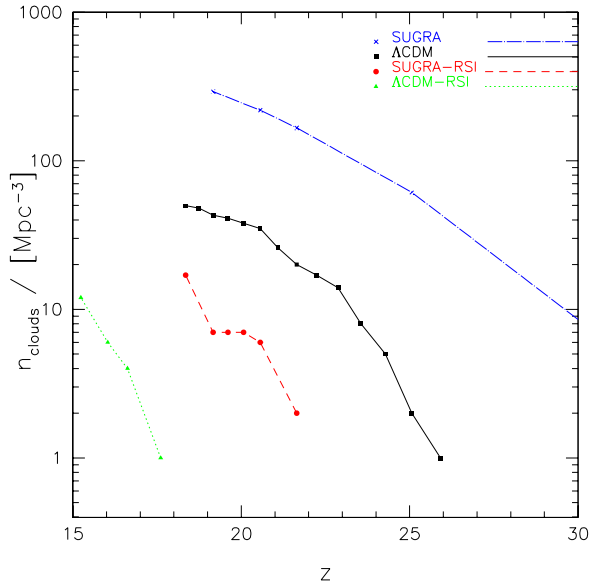


**Figure 5.** Number of clouds per unit comoving volume as function of redshift for SUGRA,  $\Lambda$ CDM, SUGRA-RSI and  $\Lambda$ CDM-RSI, as labelled.

RSI. Also, the formation of the first gas clouds strongly depends on the cosmological parameters. It happens much before  $z = 30$  for SUGRA, while it is  $z \simeq 18$  for  $\Lambda$ CDM-RSI. The reason for this pronounced difference is the integral nature of the observable  $n_{\text{clouds}}$  considered here. The production rate of clouds per unit time is the key quantity, which differs between the cosmologies considered because of the different expansion histories and primordial power spectra. The SUGRA model produces clouds earliest, followed by  $\Lambda$ CDM, while the same models with RSI stay in the same order but the structure formation process is delayed because of the modified primordial power. The integrated cloud count  $n_{\text{clouds}}$  accumulates these differences during the whole epoch of cloud production.

Finally, we have to notice that in our study we neglected the feedback effects which might influence the structure formation history of primordial clumps. For example, radiative feedbacks, such as photoionisation or molecule photo-dissociation, could stop cooling suppressing the formation of small objects; mechanical feedbacks and shocks can determine gas removal from the structure, on one hand, or induce further shell fragmentation, on the other hand. Many studies on this subject are present in the literature (see the corresponding discussion in Ciardi & Ferrara 2005, and references therein), but up to now comprehensive conclusions have not been reached: in fact the variety of approaches, approximations and parametrizations adopted by different authors leads to results which are often discordant.

## 4.2 Clumping factor and recombination time

Following Hernquist & Springel (2003), we adopt a simple statistical description of the reionisation process. Noting that each ionising photon emitted is either absorbed by a newly ionised or by a recombining hydrogen atom, the filling factor  $Q(t)$  of regions of ionised hydrogen at any given time  $t$  follows from subtracting the total number of recombinations per atom from the total number of ionising photons per hydrogen atom emitted before  $t$ . In this way, it is possible to derive a simple differential equation describing

the transition from the neutral to the completely reionised universe (Madau et al. 1999),

$$\frac{dQ}{dt} = \frac{\dot{n}_{\text{ion}}}{\bar{n}_H} - \frac{Q}{t_{\text{rec}}}, \quad (6)$$

where  $\bar{n}_H$  represents the mean comoving density of hydrogen atoms and  $\dot{n}_{\text{ion}}$  is the comoving emission rate of photons capable of ionising hydrogen. The recombination time of hydrogen,  $t_{\text{rec}}$ , is

$$t_{\text{rec}} = \frac{1}{\alpha_B C \bar{n}_H (1+z)^3 (1+2\chi)}, \quad (7)$$

where  $\alpha_B$  the recombination coefficient and  $\chi$  is the relative abundance of helium with respect to hydrogen. The dimensionless clumping factor  $C$  of hydrogen is given by

$$C \equiv \frac{\langle n_{H^+}^2 \rangle}{\langle n_{H^+} \rangle^2}. \quad (8)$$

It is evident from Eq. (7) that the recombination time is a function of redshift. Assuming a gas temperature of  $10^4$  K above which line cooling by atomic hydrogen becomes efficient, the previous relation can be written as

$$t_{\text{rec}}(z) \simeq \frac{5.88 \times 10^5}{(1+z)^3} \frac{1}{C(z)} \text{ Myr} \quad (9)$$

(Madau et al. 1999).

The left panel in Fig. 6 shows the redshift evolution of the clumping factor  $C$ , which has been estimated in our SPH simulations to be

$$C = \frac{\sum_i m_i \rho_i^{-1} \sum_j m_j \rho_j}{\left(\sum_k m_k\right)^2} \quad (10)$$

(Springel & Hernquist 2003). To avoid numerical artifacts produced by gas particles belonging to formed objects which would artificially increase the value of  $C$  due to their high density, the sum extends over all gas particles whose density  $\rho_i$  is smaller than a given threshold. In order to bracket realistic values for the threshold, we show the results (by shaded regions) assuming a maximum overdensity in the range between 100 and 500. We tested that the following analysis depends only slightly on the exact threshold.

In general the growth of  $C$  with time is quite regular for all models. For this reason we decided to fit its behaviour assuming a parabolic relation,  $C = a_0 + a_1 z + a_2 z^2$ . The resulting best-fitting parameters  $a_i$ , obtained using for  $C$  the central values of the shaded regions with the corresponding dispersion, are reported in Table 1. Notice that the relation for the  $\Lambda$ CDM-RSI model is valid only for  $z < 22$ , because of the strong flattening at higher redshifts. In line with our previous results, we find that gas clumping decreases from SUGRA through  $\Lambda$ CDM, SUGRA-RSI and  $\Lambda$ CDM-RSI. The dominant effect is caused by the shape of primordial power spectrum. In fact, the differences between the two RSI models are very small at all redshifts, where  $C$  is always between unity (corresponding to an almost perfectly smooth gas distribution), and three. For the  $\Lambda$ CDM model instead, the clumping factor starts to significantly deviate from unity at  $z \simeq 25$ , reaching four at  $z \sim 18$ . As mentioned before, the gas distribution appears much more clumpy in SUGRA, where  $C$  starts to grow already from  $z \simeq 30$ , reaching  $C \sim 6$  at  $z \simeq 19$ . Notice that our values for  $C$  in  $\Lambda$ CDM are larger by 50 per cent compared to those obtained for the same model by Springel & Hernquist (2003) (see the open squares and the dashed line in the plot). This discrepancy is caused both by the higher resolution of our simulation and by the different treatment of the gas component in the numerical code. Even if star formation is not

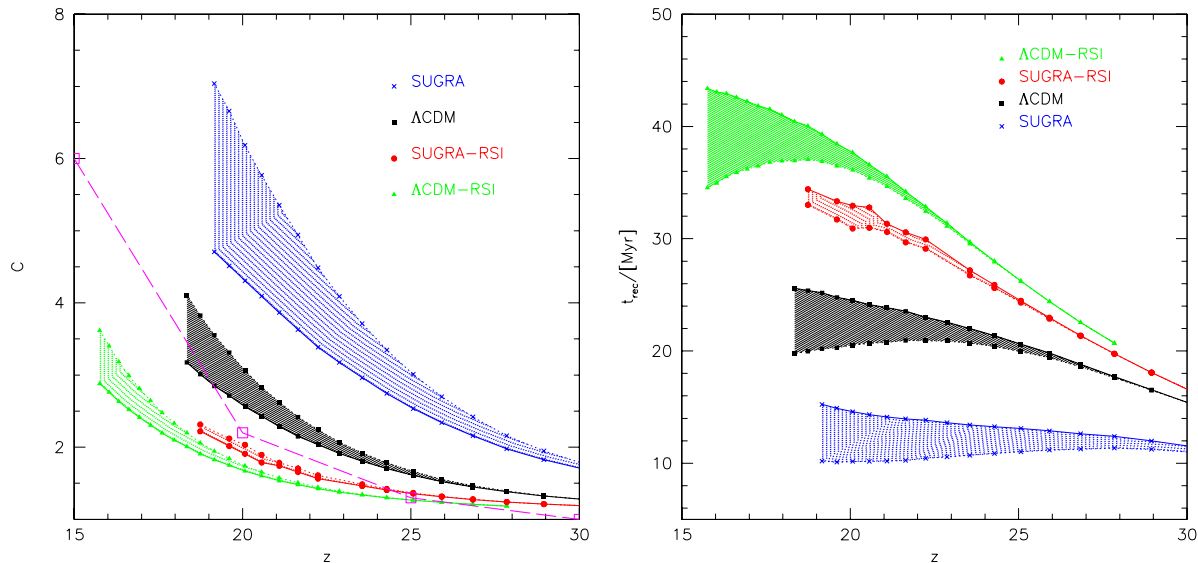


**Figure 6.** *Left panel:* The redshift evolution of the clumping factor  $C$  is shown for the different models (SUGRA,  $\Lambda$ CDM, SUGRA-RSI and  $\Lambda$ CDM-RSI from top to bottom). The shaded regions represent the uncertainty due to different choices for the maximum overdensity (here assumed between 100, dotted lines, and 500, solid lines; see the text for more detail). For reference, open squares and the dashed line show the results obtained for the Z4 model in Springel & Hernquist (2003). *The right panel* shows the evolution of the recombination time  $t_{\text{rec}}$  in Myr for the same models.

**Table 1.** The fitting parameters for the redshift evolution of the clumping factor  $C$  computed in the different simulations (listed in Column 1). We adopt a parabolic relation, given by  $C = a_0 + a_1 z + a_2 z^2$ .

Model	$a_0$	$a_1$	$a_2$
SUGRA	30.379	-1.858	0.030
$\Lambda$ CDM	17.295	-1.093	0.019
SUGRA-RSI	9.592	-0.585	0.010
$\Lambda$ CDM-RSI	20.086	-1.655	0.037

included like in Springel & Hernquist (2003), the fluid quantities (density, temperature and chemical abundances) are accurately and self-consistently evolved in our simulations, in particular also the cooling by molecular hydrogen. Thus, they are expected to produce a more realistic gas distribution in the diffuse intergalactic medium.

Knowing the clumpiness factor  $C$ , it is easy to estimate the recombination time  $t_{\text{rec}}$  from Eq. (9). The corresponding results are plotted in the right panel of Fig. 6. Of course, the maximum is obtained for the model with the lowest  $C$ , i.e.  $\Lambda$ CDM-RSI, in which the recombination process requires the long time of almost 40 Myr at  $z \simeq 18$ . The values for  $t_{\text{rec}}$  slightly decrease to about 30 Myr for SUGRA-RSI and to 20 Myr for  $\Lambda$ CDM at the same redshift, and to less than 10 Myr at  $z \simeq 19$  for SUGRA model. The differences in both  $C$  and  $t_{\text{rec}}$  are again spread over almost an order of magnitude because they are integrated observables like  $n_{\text{clouds}}$ .

## 5 IMPLICATIONS FOR REIONISATION

It is interesting to draw consequences from our results regarding the phenomenology of the overall reionisation process, checking in particular how these scenarios might be constrained by data on the reionised optical depth. Even if more accurate and quantitative estimates would require detailed simulations including radiative transfer, we can reliably discuss the problem of reionisation based on preceding work.

We first need a relation between the reionisation epoch and the total Thomson optical depth  $\tau$ , which can be derived from the CMB data. To compare the WMAP results to the predictions for the cosmological model here considered, we compute the redshift evolution of  $\tau$ , adopting a simple model which assumes that complete reionisation occurs instantaneously at a some redshift  $z$ . The differential Thomson optical depth for complete ionisation is given by

$$d\tau(z) = \frac{n(z)\sigma_T c}{(1+z)H(z)} dz, \quad (11)$$

where

$$\sigma_T = \frac{8\pi}{3} \left( \frac{e^2}{m_e c^2} \right)^2 \approx 6.65 \times 10^{-25} \text{ cm}^2 \quad (12)$$

is the Thomson cross section,  $c$  is the speed of light and  $H(z)$  is Hubble parameter at  $z$ . The mean electron number density is given in terms of the ionisation fraction  $x_e(z)$  by  $n(z) = n(z=0)(1+z)^3 x_e(z)$ . Notice that in the previous equations the only dependence on the cosmological model appears in  $H(z)$  through the Hubble constant and the expansion rates. For this reason the optical depth is completely independent on the spectral parameters (such as the power-spectrum index  $n$ ), and the RSI predictions agree exactly with the corresponding  $n = 1$  model.

The integrated optical depth, computed assuming  $x_e = 1$  always, is shown in Fig. 7 for both  $\Lambda$ CDM and SUGRA with  $w_0 = -0.85$ . The horizontal dotted lines represent the observa-



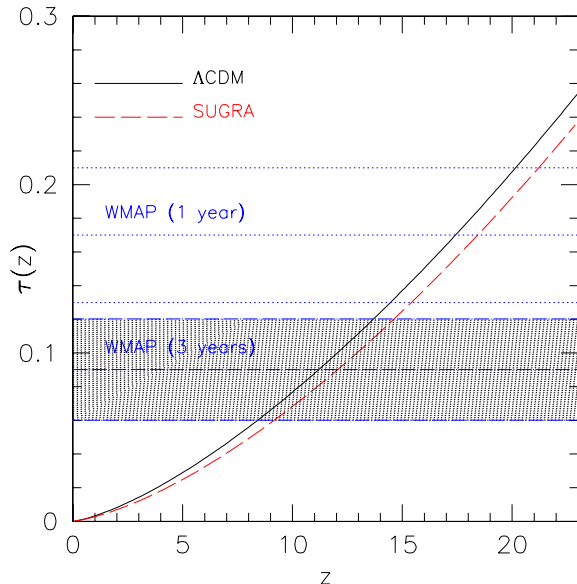


**Figure 7.** The integrated Thompson optical depth  $\tau$  for  $\Lambda$ CDM (solid line) and SUGRA model with  $w_0 = -0.85$  (long-dashed line) are compared to the WMAP constraints: first-year and three-years results are shown by the regions within the dotted lines and by the shaded region, respectively.

tional estimate (with its  $1-\sigma$  error bars) obtained from the first-year WMAP data (Kogut et al. 2003), while the shaded region shows the more recent values from the three-year WMAP data (Page et al. 2006).<sup>2</sup> When compared to standard  $\Lambda$ CDM, SUGRA has a lower optical depth, with a difference of about  $\Delta\tau = 0.02$  at  $z \simeq 17$  and  $\Delta\tau = 0.01$  at  $z \simeq 10$ . As expected, this implies an earlier reionisation epoch, causing tension between the present model and the measured reionisation optical depth (Spergel et al. 2006), in addition to that regarding other cosmological probes (see, e.g., Spergel et al. 2003; Knop et al. 2003; Riess et al. 2004). Although a more accurate estimate would require a realistic description of the reionisation history, which in turn strongly depends on the free parameters of the adopted modelling, we can then assume that the reionisation in both models ( $\Lambda$ CDM and SUGRA) must occur and conclude at early epoch, ranging between  $z \simeq 15$  and  $z \simeq 10$ , to agree with the measured optical depth within  $1-\sigma$ . In general, these results demonstrate that the records of the high-redshift expansion rate in the physics of the primordial gas clouds may be used to constrain the dark energy from reionisation data. Mainini et al. (2003) came to similar conclusions without considering modifications to the physics of gas clouds.

We can now study in more detail how the reionisation process is going on in the redshift range covered by our simulations. First, we compute the total number of ionising photons  $n_{\text{ion}}$ . For this goal, we can follow the usual ‘one star per halo’ assumption for mini-halos (see, e.g., Yoshida et al. 003a,b) and safely use the cloud number as a good approximation for the number of very massive stars: in fact strong radiative feedback disfavours the formation of multiple stars inside each primordial gas cloud. Then we set the mass of a Pop III star to be  $500 M_{\odot}$  and we use the tables in Schaerer (2002) to estimate its lifetime ( $\sim 1.9$  Myr) and the mean

ionising flux along the evolutionary track ( $\sim 6.8 \times 10^{50}$  photons per second). We also assume an optimistic constant photon escape fraction of unity, which, however, can be considered realistic when the gas distribution is reasonably smooth (Oh et al. 2001). Detailed calculations by Kitayama et al. (2004) indeed find that such a large escape fraction is plausible for small mass haloes. In order to complete the reionisation process, the resulting values for  $n_{\text{ion}}$  must be at least as large as the total number of hydrogen atoms in the simulation volume, which in our case corresponds to  $n_{\text{tot}} \sim 4 \times 10^{66}$ . In Fig. 8 the dashed lines show the redshift evolution for  $n_{\text{ion}}$  for the different models. We notice that only the SUGRA model is able to produce a sufficient number of ionising photons in the redshift range considered by our simulations, while for all remaining models the ratio  $n_{\text{ion}}/n_{\text{tot}}$  is smaller than unity. In particular the two RSI models at the final simulation outputs reach only the 10-15 per cent of the required photons.

Second, we have to consider that, as discussed before, recombination is counteracting the reionisation process. Using the values for the clumping factor and recombination time accurately derived from the simulations (and shown in Fig. 6), we can easily compute the cumulative number of recombined atoms, numerically solving Eq. (6). The results are also displayed in Fig. 8, where the shaded regions correspond to the uncertainties for  $C$  and  $t_{\text{rec}}$  discussed in the previous section. The plot is suggesting that the recombination process is rapid enough to significantly affect the fraction of ionised atoms. At the final simulation outputs, we find that the ratio between recombined and ionised atoms is about 75 per cent for SUGRA and  $\Lambda$ CDM, and about 25 for the two RSI models.

Our analysis suggests that all models here considered, with the exception of SUGRA, are producing an insufficient number of collapsed objects to achieve complete reionisation in the redshift interval covered by the simulations. This is true not only for both RSI models, whose suppression of small scale power prevents the reionisation, but also for the standard  $\Lambda$ CDM model. These conclusions are in qualitative agreement with the previous analysis performed by Yoshida et al. (003b), who, considering a simple model based on the formation of first stars in mini-haloes by molecular cooling, demonstrated that complete reionisation is reached when a density of  $50 \sim 100$  very massive stars per comoving  $\text{Mpc}^3$  is turned on per  $\sim 1$  recombination time (see also Yoshida et al. 003a,c). We notice that for these models the results are not conflicting with the three-year WMAP data which suggest a later reionisation epoch compared to the first-year analysis. Allowing the simulations to evolve up to  $z \simeq 10$  would certainly increase both the number of gas clouds and the clumpiness, completing the reionisation process.

Finally, we notice that for the formation and evolution of cosmic structures in SUGRA are so fast that the corresponding number of gas clouds is so large and  $t_{\text{rec}}$  so low that a global reionisation is expected at redshifts even higher than  $z = 20$ . As mentioned already, this anticipation of the reionisation epoch could be in conflict with observations (see, e.g., the contour levels in Fig. 3 of Spergel et al. 2006), indicating the potential constraining power of the dark energy records in the formation of primordial gas clouds which we pointed out in this work.

## 6 CONCLUSIONS

We presented hydrodynamic N-body simulations of the formation of primordial gas clouds on scales of tens of kpc in a variety of cosmological models, characterised by different dynamics in the dark-energy component. Our main results are that the records of

<sup>2</sup> We have to notice that our results for  $\tau$  must be considered as an extrapolation at redshifts higher than the reionisation epoch suggested by WMAP: since  $x_e$  vanishes, the curves should indeed display a horizontal floor.

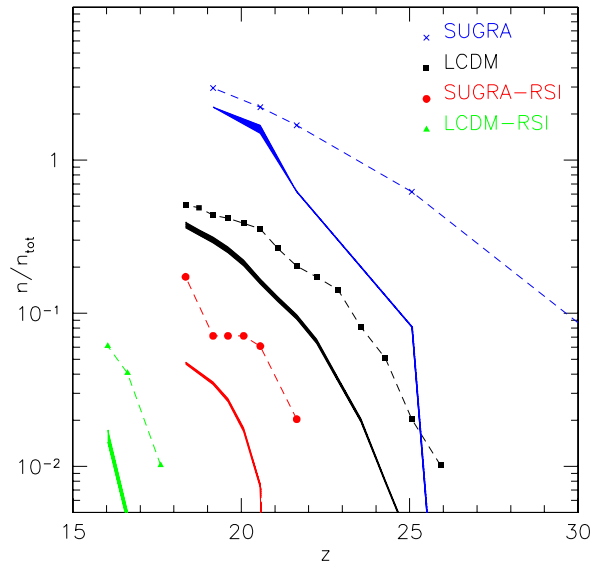


**Figure 8.** The redshift evolution of the number of ionizing photons  $n_{\text{ion}}$  (dashed lines) and recombined atoms (shaded regions corresponding to the uncertainties for  $t_{\text{rec}}$  displayed in the right panel of Fig. 6) are shown for the different models (SUGRA,  $\Lambda$ CDM, SUGRA-RSI and  $\Lambda$ CDM-RSI from top to bottom). Both quantities are normalized to the total number of atoms  $n_{\text{tot}}$  (see more detail in the text).

the modified expansion rate are well evident in the population and the clumpiness of such clouds. Cosmological models with the same power-spectrum normalisation at present show earlier cloud formation if the dynamics of the dark energy is enhanced, represented by an equation of state parameter  $w > -1$  as in quintessence models.

Within dark energy models compatible with the present data on cosmic microwave background and large scale structure, the difference in the integral population of clouds may vary by up to an order of magnitude, as a consequence of the different differential efficiency for structure formation. This is consistent with earlier results indicating a higher concentration in dark matter haloes under similar conditions (Dolag et al. 2004).

Since abundance and clumpiness of structures are directly related to the amount of primordial power on the corresponding scales, we varied the shape of the primordial power spectrum by a running spectral index reducing power on small scales within the confidence level of the three-years WMAP data (Spergel et al. 2006). As expected, we find that the extra population and clumpiness of clouds produced by a higher dark energy abundance compared with its level today might be mitigated if the primordial spectral index is running, decreasing the power on small scales.

Adopting a simple picture for the reionisation process, we derived consequences for the reionisation itself, leading to an earlier beginning of the reionisation process in models where cloud formation starts earlier. On the basis of these results, we are able to identify possible tension between the WMAP data on the reionisation optical depth and cosmological models whose dark energy is as dynamical as in SUGRA quintessence models.

Our results demonstrate that the effects on cosmological structure formation from a modified expansion history through different dark energy models must be traced back to the formation of the first clouds. In turn, this means that constraints on the dark energy, and in particular its abundance at high redshifts, may be obtained by

forthcoming experiments aiming at measuring the abundance and the clumpiness of primordial gas clouds. In particular, the Atacama Large Millimeter Array (ALMA<sup>3</sup>) and the Mileura Widefield Array (MWA<sup>4</sup>) will probe the early stages of structure formation, say between  $z = 6$  and 10, where the reionization in progress should keep a record of the population of reionizing primordial gas clouds.

## ACKNOWLEDGEMENTS

Computations were performed on the IBM-SP4/5 at CINECA, Bologna, with CPU time assigned under an INAF-CINECA grant, and the IBM-SP4 at the computer centre of the Max Planck Society with CPU time assigned to the Max Planck-Institut für Astrophysik. We are grateful to C. Gheller for his assistance. We acknowledge useful discussions with Benedetta Ciardi, Bepi Tormen and Licia Verde.

## REFERENCES

- Abel T., Anninos P., Zhang Y., Norman M. L., 1997, *New Astronomy*, 2, 181
- Anninos P., Zhang Y., Abel T., Norman M. L., 1997, *New Astronomy*, 2, 209
- Astier P., et al., 2006, *A&A*, 447, 31
- Bagla J. S., Prasad J., 2006, *MNRAS*, 370, 993
- Bartelmann M., Meneghetti M., Perrotta F., Baccigalupi C., Moscardini L., 2003, *A&A*, 409, 449
- Battye R. A., Weller J., 2003, *Phys. Rev. D*, 68, 083506
- Bond J. R., Cole S., Efstathiou G., Kaiser N., 1991, *ApJ*, 379, 440
- Brax P., Martin J., 2000, *Phys. Rev. D*, 61, 103502
- Brax P. H., Martin J., 1999, *Physics Letters B*, 468, 40
- Ciardi B., Ferrara A., 2005, *Space Science Reviews*, 116, 625
- Ciardi B., Ferrara A., White S. D. M., 2003, *MNRAS*, 344, L7
- Cole S., et al., 2005, *MNRAS*, 362, 505
- Desjacques V., Nusser A., 2005, *MNRAS*, 361, 1257
- Dolag K., Bartelmann M., Perrotta F., Baccigalupi C., Moscardini L., Meneghetti M., Tormen G., 2004, *A&A*, 416, 853
- Galli D., Palla F., 1998, *A&A*, 335, 403
- Gao L., White S. D. M., Jenkins A., Frenk C. S., Springel V., 2005, *MNRAS*, 363, 379
- Haiman Z., Mohr J. J., Holder G. P., 2001, *ApJ*, 553, 545
- Heitmann K., Lukić Z., Habib S., Ricker P. M., 2006, *ApJ*, 642, L85
- Hernquist L., Springel V., 2003, *MNRAS*, 341, 1253
- Jang-Condell H., Hernquist L., 2001, *ApJ*, 548, 68
- Jenkins A., Frenk C. S., White S. D. M., Colberg J. M., Cole S., Evrard A. E., Couchman H. M. P., Yoshida N., 2001, *MNRAS*, 321, 372
- Kitayama T., Yoshida N., Susa H., Umemura M., 2004, *ApJ*, 613, 631
- Klypin A., Macció A. V., Mainini R., Bonometto S., 2003, *ApJ*, 599, 31
- Knop R. A., et al., 2003, *ApJ*, 598, 102
- Kogut A., et al., 2003, *ApJS*, 148, 161
- Madau P., Haardt F., Rees M. J., 1999, *ApJ*, 514, 648
- Mainini R., Colombo L. P. L., Bonometto S. A., 2003, *New Astronomy*, 8, 751

<sup>3</sup> [www.eso.org/projects/alma/science/](http://www.eso.org/projects/alma/science/)

<sup>4</sup> [www.haystack.mit.edu/ast/arrays/mwa/site/index.html](http://www.haystack.mit.edu/ast/arrays/mwa/site/index.html)

- Majumdar S., Mohr J. J., 2003, *ApJ*, 585, 603
- Meneghetti M., Bartelmann M., Dolag K., Moscardini L., Perrotta F., Baccigalupi C., Tormen G., 2005, *A&A*, 442, 413
- Oh S. P., Nollett K. M., Madau P., Wasserburg G. J., 2001, *ApJ*, 562, L1
- Page L., et al., 2006, preprint, astro-ph/0603450
- Peebles P. J., Ratra B., 2003, *Reviews of Modern Physics*, 75, 559
- Press W. H., Schechter P., 1974, *ApJ*, 187, 425
- Reed D., Gardner J., Quinn T., Stadel J., Fardal M., Lake G., Governato F., 2003, *MNRAS*, 346, 565
- Riess A. G., et al., 2004, *ApJ*, 607, 665
- Schaerer D., 2002, *A&A*, 382, 28
- Seljak U., et al., 2005, *Phys. Rev. D*, 71, 103515
- Seljak U., Slosar A., McDonald P., 2006, preprint, astro-ph/0604335
- Sheth R. K., Tormen G., 1999, *MNRAS*, 308, 119
- Sheth R. K., Tormen G., 2002, *MNRAS*, 329, 61
- Sokasian A., Abel T., Hernquist L., Springel V., 2003, *MNRAS*, 344, 607
- Sokasian A., Yoshida N., Abel T., Hernquist L., Springel V., 2004, *MNRAS*, 350, 47
- Somerville R. S., Bullock J. S., Livio M., 2003, *ApJ*, 593, 616
- Spergel D. N., et al., 2003, *ApJS*, 148, 175
- Spergel D. N., et al., 2006, preprint, astro-ph/0603449
- Springel V., 2005, *MNRAS*, 364, 1105
- Springel V., et al., 2005, *Nature*, 435, 629
- Springel V., Hernquist L., 2003, *MNRAS*, 339, 312
- Springel V., Yoshida N., White S. D. M., 2001, *New Astronomy*, 6, 79
- Tegmark M., et al., 2004, *Phys. Rev. D*, 69, 103501
- Viel M., Haehnelt M. G., 2006, *MNRAS*, 365, 231
- Viel M., Haehnelt M. G., Lewis A., 2006, *MNRAS*, 370, L51
- Viel M., Weller J., Haehnelt M. G., 2004, *MNRAS*, 355, L23
- Wang L., Steinhardt P. J., 1998, *ApJ*, 508, 483
- Warren M. S., Abazajian K., Holz D. E., Teodoro L., 2006, *ApJ*, 646, 881
- Wyithe J. S. B., Loeb A., 2003, *ApJ*, 588, L69
- Yoshida N., Abel T., Hernquist L., Sugiyama N., 2003a, *ApJ*, 592, 645
- Yoshida N., Sokasian A., Hernquist L., Springel V., 2003b, *ApJ*, 598, 73
- Yoshida N., Sokasian A., Hernquist L., Springel V., 2003c, *ApJ*, 591, L1
- Zaroubi S., Viel M., Nusser A., Haehnelt M., Kim T.-S., 2006, *MNRAS*, 369, 734